Assimilation of Airborne Imagery with a Wave Model for Bathymetric Estimation

Author(s): Chadwick L. Monfort and Thomas C. Lippmann
Source: Journal of Coastal Research, :40-49.
Published By: Coastal Education and Research Foundation
DOI: http://dx.doi.org/10.2112/SI_62_5
URL: http://www.bioone.org/doi/full/10.2112/SI_62_5

Journal of Coastal Research	SI	62	40–49	West Palm Beach, Florida	Spring 2011

Assimilation of Airborne Imagery with a Wave Model for Bathymetric Estimation

Chadwick L. Monfort*† and Thomas C. Lippmann‡

†Byrd Polar Research Center
Ohio State University
Columbus, OH 43210, U.S.A.

‡Center for Coastal and Ocean Mapping
University of New Hampshire
Durham, NH 03824, U.S.A.
lippmann@ccom.unh.edu

www.cerf-jcr.org

ABSTRACT

MONFORT, C.L. and LIPPMANN, T.C., 2011. Assimilation of airborne imagery with a wave model for bathymetric estimation. *In:* Pe'eri, S. and Long, B. (eds.), *Applied LIDAR Techniques*, Journal of Coastal Research, Special Issue No. 62, 40–49. West Palm Beach (Florida), ISSN 0749-0208.

One of the most useful survey methods in nearshore studies is airborne light detection and ranging (LIDAR), which is able to densely sample topographic and shallow bathymetric elevation data over large geographic regions. Airborne LIDAR bathymetry systems are dependent on water clarity, but in the surf zone sediment and air bubbles entrained in the water column by wave breaking attenuate the laser pulse and compromise the LIDAR's ability to retrieve accurate bottom elevations. Data assimilation techniques can improve the ability of LIDAR systems to estimate bathymetry inside the surf zone. The assimilation methods are based on comparing pixel intensity patterns (scaled by offshore wave energy flux) extracted from time-averaged airborne imagery with dissipation profiles produced by a simple wave-energy transformation model. The subaerial topography and the offshore bathymetry are assumed known and an initial featureless bathymetry is assumed in the surf zone (where the data are missing). Differences between modeled dissipation and observed image pixel intensity patterns can be minimized by incrementally modifying the bathymetry. Final assimilated bathymetry estimates are compared with surveyed bathymetric data collected at the U.S. Army Corps of Engineers Field Research Facility in Duck, NC using traditional surveying methods. Analysis of data from three aerial overflights produced average root mean square differences between assimilated and surveyed bathymetry of 25–35 cm, similar to results from land-based systems. This methodology can be used to improve LIDAR-derived profiles where large gaps exist because of surf that attenuates the laser pulses, and allow for more complete evaluation of large-scale coastal behavior that includes profile evolution within the surf zone.

ADDITIONAL INDEX WORDS: *Beach profiles, LIDAR, large-scale coastal behavior, airborne video, image mosaic, wave-energy transformation.*

INTRODUCTION

The primary mechanism for coastal sediment transport and erosion is the energy dissipated by waves and the currents they produce as they progress shoreward through the surf zone. Wave dissipation is difficult to directly measure, but can indirectly be modeled if the underlying bathymetry is known (*e.g.,* Lippmann, Brookins, and Thornton, 1996a; Thornton and Guza, 1983; and many others). In the shallow nearshore region (within a few hundred meters of the shoreline), the bathymetry largely dictates wave transformation, the spatial distribution of currents, and is thus of order one importance to modeling nearshore sediment transport and beach evolution.

The complex nature of the near shore, along with its tendency to develop rapidly over large spatial scales, makes it a very difficult region in which to measure bathymetry. Traditional methods utilize global positioning systems (GPS) and sonar altimeters onboard mobile platforms, but can only be applied to relatively small areas because these techniques are labor intensive and are often limited by surf-zone conditions. Variations in coastal change occur over scales on the order of 10s to 100s of kilometers, limiting application of traditional methods. The ability to collect accurate bathymetry over large spatial regions is essential for quantifying large-scale sediment transport, determining areas of coastlines at risk to erosion and storm damage, and for general research of large-scale coastal behavior (LSCB).

Advancements in GPS and inertial navigation systems (INS) technology have led to the development of airborne light detection and ranging (LIDAR; Irish, McClung, and Lillycrop, 2000). An airborne LIDAR system works by transmitting laser pulses from an aircraft at an extremely high frequency (ranging about 135 to 3000 Hz) and measuring their response waveform that is subsequently interrogated for estimating reflective ground surfaces (Guenther, 2001). In optimal conditions, using the travel time from emission to return of each laser pulse, together with accurate orientation information provided by an integrated GPS/INS system, LIDAR can define ground elevations within ±2 m horizontally ±15 cm vertically (Irish, McClung, and Lillycrop, 2000).

DOI:10.2112/SI_62_5 received and accepted in revision 13 September 2010.

*Present address: Planning Systems, Inc., 3990 Old Town Avenue, San Diego, CA 92110, U.S.A.

Using a green wavelength laser to penetrate the water column, bathymetric LIDAR is also able to collect submarine topographic data with limitations depending on water clarity and depth. Airborne LIDAR has the capability to accurately sample large geographic areas in relatively short periods of time, making it ideal for large-scale studies of coastal regions. LIDAR is currently being used for coastal mapping and storm impact studies throughout North America but only provides bathymetry in regions where water clarity allows seabed detection.

In the surf zone, air bubbles and sediment entrained in the water column impede the ability of bathymetric LIDARs to accurately obtain sea-bottom elevation data. The surf zone plays an important role in wave energy dissipation and limits the usefulness of airborne LIDAR bathymetry (ALB). Current ALB systems must either wait for deployment during calm wave conditions to avoid this issue or are restricted to collecting data seaward of the surf zone. It would be advantageous to both industry and science with interests in LSCB to improve the capabilities of estimating bathymetry data in the surf zone. Of high interest is the fusion of electro-optical sensors (*e.g.,* video and hyperspectral cameras) with incomplete ALB profiles to improve spatial coverage inside the surf zone.

Data assimilation methods have been established for estimating bathymetry in the surf zone using known offshore wave conditions and time-averaged imagery obtained from land-based video systems (Aarninkhof and Ruessink, 2004; Aarninkhof, Ruessink, and Roelvink, 2005; Van Dongeren *et al.*, 2008). Data assimilation techniques are based on the principles of conservation of wave energy. As a wave breaks in the surf zone, the wave dissipates its energy through turbulent processes. On typical sandy beaches, dissipation by bottom friction is considered negligible and energy loss due to wave breaking is the primary dissipative mechanism (Thornton and Guza, 1983). Wave models can estimate the distribution of wave dissipation but only if the beach profile is known. In the case of ALB the measured bathymetry is often incomplete, and as a consequence dissipation patterns in the nearshore cannot be calculated. Assimilation techniques are able to iteratively estimate bathymetric profiles when they are not available by utilizing spatial dissipation information obtained from time-averaged imagery of surf zone wave-breaking patterns. Previous work using data assimilation techniques has concentrated on creating time-averaged mosaics from video data collected by an obliquely oriented land-based camera. In this work, image data collected from a downward-looking video camera mounted on an airplane were utilized.

In the following, we describe the methodologies leading to estimation of bathymetry inside the surf zone where only profile data are known on the subaerial beach and seaward of the surf zone. We first describe our field methods for obtaining airborne imagery and creating time-average mosaics used for estimating the spatial distribution of wave dissipation, and include a description of the field site where the ground-truth bathymetry and input wave data were obtained. We then present the wave model used to estimate wave dissipation across arbitrary beach profiles, followed by a discussion of our assimilation techniques for estimating profiles from image mosaics and the wave model. Results are presented and discussed in terms of application limitations and sources of error. Finally , conclusions are drawn and presented.

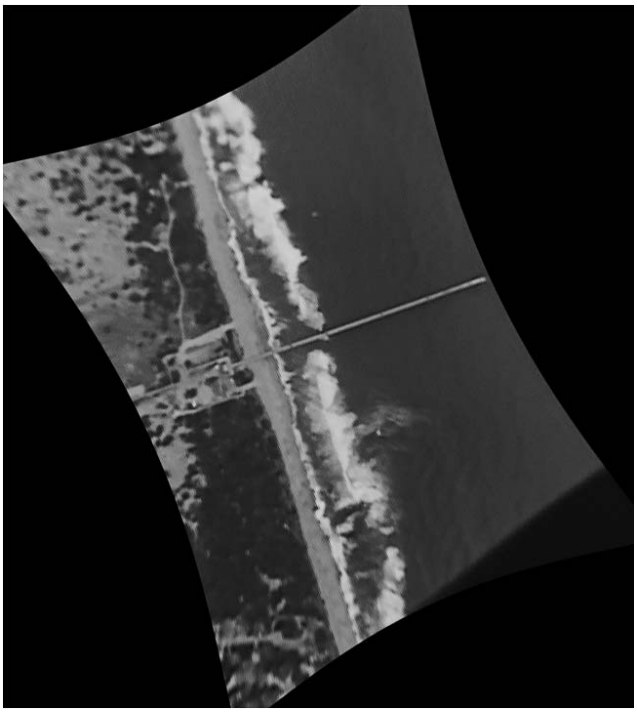

Figure 1. Single-frame image, with lens distortion removed, obtained by the AVS system over the FRF study site. Each individual video image was transformed to orthonormal geodetic ground coordinates at sea level (Holland *et al.*, 1997). All the video images overlapping an area were added numerically to create a time-averaged mosaic. Typical number of overlapping images per mosaic is 900–1350 images (duration time of 30–45 s).

FIELD METHODS

Image data were obtained from overflights along the Outer Banks of North Carolina using the aerial video system (AVS) (Figure 1; Worley *et al.*, 1997, 1998). The AVS has been used to create time-averaged image mosaics from overflights spanning 100–200 km of coastline, and subsequently to analyze large-scale changes in sand bar position as a function of alongshore distance and shoreline change (Kannan, Lippmann, and List, 2003; Lippmann and Kannan, 2003; Lippmann, List, and Kannan, 2003). Aerial video system overflights were generally conducted at an altitude of 300–600 m at a speed-over-ground of 80–90 knots. The camera field of view varied depending on altitude. In all cases a 4.5-mm, wide-angle, fixed-focal length, auto-iris lens was used. Typical dwell time for any feature in the image was about 30–45 seconds, again depending on altitude and aircraft speed. The dwell time is necessary to smooth out natural fluctuations in random wave-breaking events, but is much less than typically used for land-based systems (order 10 min).

The system contains a downward-looking 2/3 inch (16.9 mm) charge-coupled device Sony monochrome video camera that records video on tape at 30 Hz. Video data is later digitized in the laboratory at 5 Hz with an image-digitizing module in a host personal computer running the Linux operating system. Each image is stored individually in portable grayscale format with pixel intensities ranging from 0 (black) to 255 (white). Also included is a differential GPS receiver for accurate (5–20 cm) positioning and time synchronization (1/30 second). The ephemeral GPS data are post-processed with a nearby continuously operating reference (CORS) base station at 1 Hz and interpolated to the video time series. An onboard KVH active stabilization antennae pedestal (ASAP) keeps the camera in an approximate (1–6°) downward orientation relative to nadir.

Intrinsic image orientation parameters were determined using standard laboratory techniques including the determination of tertiary image distortion parameters, image centers, and horizontal scale factors (Holland *et al.*, 1997). As the motion of the ASAP does not allow for precise estimation of pitch and roll information, the pitch and roll were assumed to be zero for each image. The behavior of the ASAP and aircraft motion is generally random about the mean look angle of the image principal axis; thus, the uncertainty in orientation induced by this assumption is generally smoothed in the time-averaging process, which resulted in a slightly blurred image. In general, the bias in pitch and roll can be removed manually by periodically comparing known ground features visible in the imagery. Biases associated with small pitch and roll can largely be ignored because their effects become minimal after averaging. In cases with large pitch and roll bias (determined qualitatively by image clarity), the data were not used.

Although the pitch and roll can generally be assumed to be zero without compromising the final time-averaged image mosaic, the rotation about the image principal axis (the yaw) cannot be as easily removed, particularly since the aircraft orientation is often "crabbing" at an angle relative to its GPS-measured flight path (that is, the flight path axis does not coincide with the aircraft body axis). To estimate the yaw of the images relative to the GPS heading information a sample set of rectified images was selected at an interval (typically every 80 images) such that a portion (typically about 20%) of each selected image overlapped. This sample data set was displayed in ArcGIS and iteratively adjusted manually until fixed features such as the shoreline and sand dune positions in the images were aligned. The yaw biases were linearly interpolated through the entire data set and applied to adjust GPS heading values.

Each image was rectified into orthonormal geodetic (universal transverse Mercator [UTM]) ground coordinates (Morris, 1966) using the GPS camera position, and intrinsic and extrinsic orientation parameters. The vertical elevation was assumed to be at mean sea level on the basis of tidal records at the time of the overflight. Pixel intensities from each rectified image were assigned a cell position within a georeferenced matrix on the basis of real-world UTM coordinates at 2-m resolution and stored as a georeferenced tiff image file. Because of the uncertainty in georectification of any particular image as well as the limited dwell time

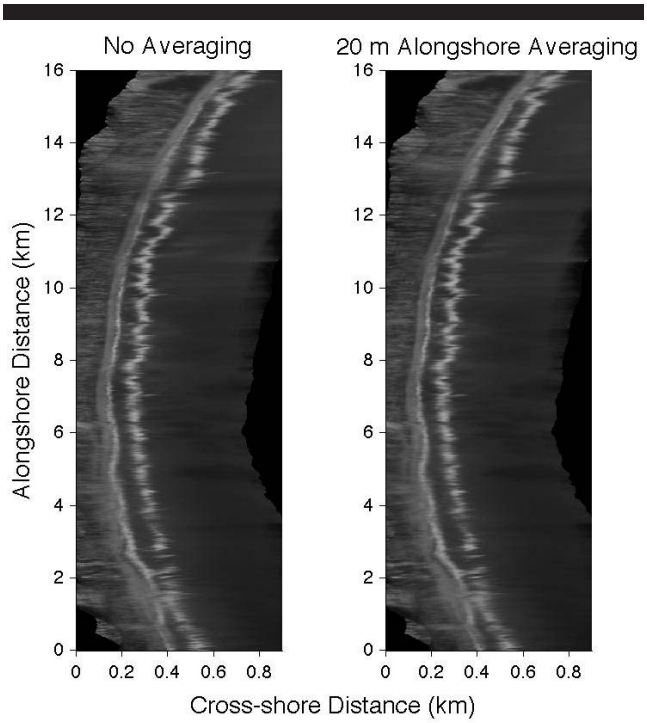

Figure 2. Time-averaged video-mosaic images obtained by the AVS system overflight along the North Carolina Outer Banks to the south of the FRF study site: (right) with a 20-m alongshore averaging and (left) without averaging (2-m by 2-m pixel resolution). The subaerial beach is located to the left and the Atlantic Ocean is located to the right in the images. The alongshore extent in the image is 16 km. The bright white bands indicate the position of wave breaking at the shoreline and over an offshore sandbar approximately 100 m from shore.

(relative to land-based systems) in the aerial overflights at any particular location, average pixel intensities were spatially averaged 20 m in the alongshore direction to further smooth wave-breaking distributions (Figure 2; Kannan, Lippmann, and List, 2003). Individual cross-shore transects of image intensity can be extracted at any given alongshore location and compared with local bathymetric data.

Ground-truth bathymetric data were obtained using the coastal research amphibious buggy (CRAB; Birkemeier and Mason, 1984) by the U.S. Army Corps of Engineers (USACE) field research facility (FRF) near the town of Duck located on the Outer Banks of North Carolina along the central eastern seaboard of the United States. The vertical accuracies of the FRF bathymetric data obtained with the CRAB were on the order of 5–10 cm (Birkemeier and Mason, 1984). The FRF bathymetric data was comprised of individual profile transects spanning a 1200-m stretch of coastline surrounding the facilities' research pier (Figure 3). Cross-shore and alongshore locations were in the local FRF coordinate system, with elevations relative to the national geodetic verical datum of 1929 (NGVD29; datum approximately at mean sea level). An airborne image mosaic overlooking the FRF from 13 April 2002 is also shown in Figure 3 with the location of FRF surveyed profile lines overlaid on the image. Image mosaics were manually checked against several GPS ground points

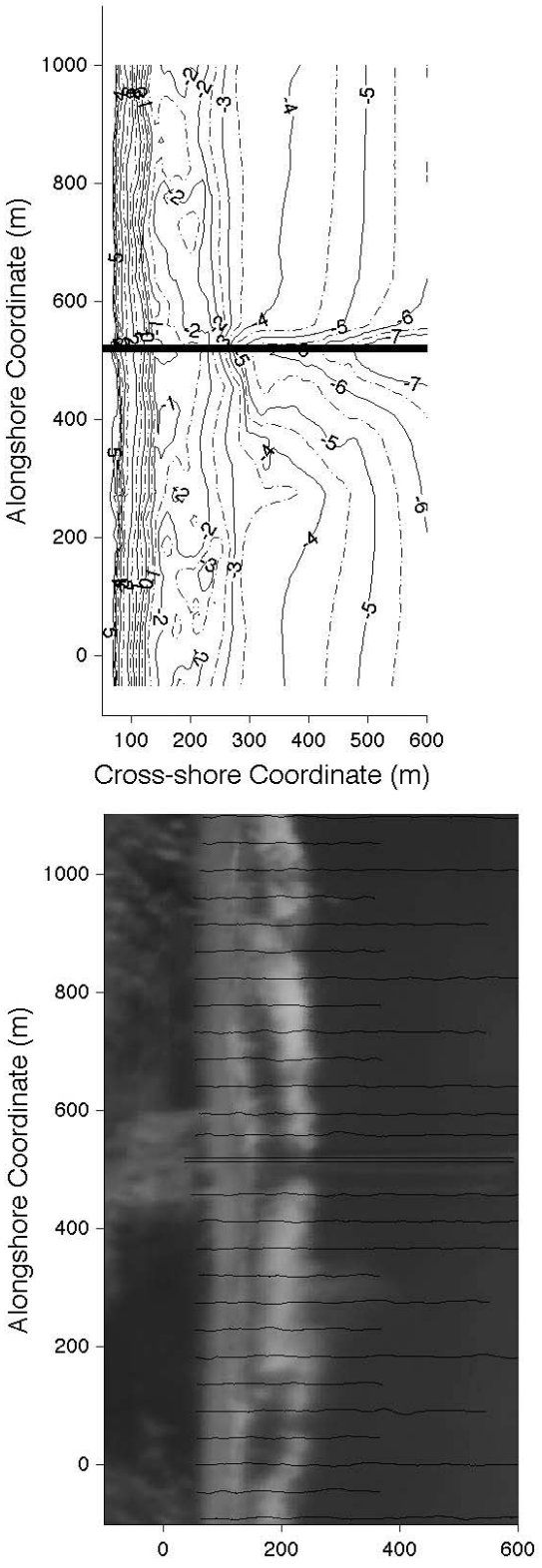

Figure 3. Bathymetric contour map of the FRF field site (top) measured on 17 April 2002. The elevation contour lines are in meters relative to NGVD29 (datum approximately at mean sea level) and the horizontal coordinates in the local FRF system. In the center of the domain is the location of the large research pier that extends over 500 m offshore. A time-averaged mosaic (bottom) over the same region obtained from an AVS overflight on 13 April 2002. The location of profile lines used in the bathymetric contour map are overlaid onto the image.

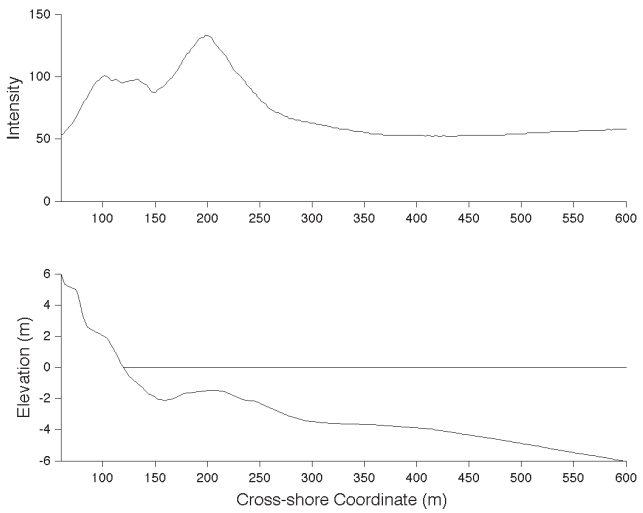

Figure 4. Example pixel intensity profile (upper panel) extracted from the time-averaged mosaic shown in Figure 2 at alongshore coordinate $y = 230$ m. The corresponding cross-shore bathymetry profile measured by the FRF at the same alongshore location is shown in the lower panel.

along the FRF pier to ensure proper alignment between the two data sets. Image intensity profiles are extracted at the location of the profile transects (Figure 4) and utilized in the assimilation procedure.

FRF profile data were synthetically modified to simulate an incomplete ALB profile by eliminating the surf zone data (Figure 5), and then used to test the assimilation procedure by assuming an initially featureless profile numerically calculated using a hyperbolic tangent equation defined by Lippmann, Herbers, and Thornton (1999):

$$h = x\tan\beta_2 + \frac{a_1}{\tan\beta_2}(\tan\beta_1 + \tan\beta_2)\tanh\left(\frac{x\tan\beta_1}{a_1}\right) \quad (1)$$

This function uses values for foreshore slope, $\beta_1 = 0.10$ rad, and offshore slope, $\beta_2 = 0.008$ rad, that are typical of beaches near the field site. A value for the coefficient a_1 is then calculated using the elevation of surveyed points just before and after the surf zone. This hyperbolic tangent function creates a featureless estimate of the surf-zone bathymetry without sand bars. The full FRF profile is then later used to evaluate the ability of the assimilation to estimate the actual bathymetry.

Tidal elevations needed to establish water levels for the wave model and in the rectification of images were obtained from a National Oceanic and Atmospheric Administration tide gauge located at the end of the FRF pier. Offshore wave height, wave angle, and spectral peak wave frequency used to

←

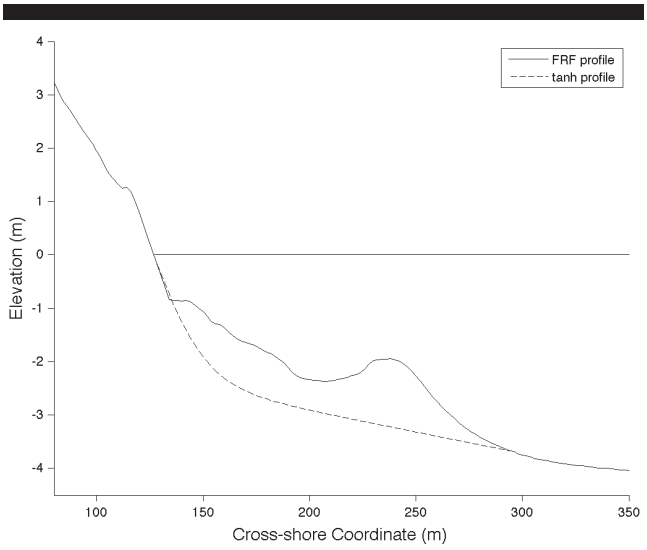

Figure 5. An example of measured (solid line) cross-shore bathymetric profile at alongshore location y = 600 m and the initial assumed (dashed line) surf-zone profile used to test the assimilation methods (on the basis of Equation [1]).

initialize the wave model were obtained from an established *in situ* pressure sensor array located in 8-m water depth at the FRF field site. Details of the FRF field site, survey methods, tide gauge, and 8-m directional array can be found at the FRF website (http://www.frf.usace.army.mil).

WAVE MODEL

This section describes the wave model used to estimate wave dissipation over arbitrary beach profiles, and follows work by Thornton and Guza (1983) and Lippmann, Brookins, and Thornton (1996a). The cross-shore wave energy flux balance can be used to model wave transformation across the surf zone,

$$\frac{\partial}{\partial x}\left(E_w c_g \cos\alpha\right) = \varepsilon_r \tag{2}$$

where x is the cross-shore location, ε_r is dissipation due to wave breaking, c_g is the wave group velocity, α is the wave angle, and $E_w = \rho g H^2/8$ is the linear theory wave energy where ρ is density, g is gravity, and H is wave height. Following LeMahaute (1962), the dissipation can be written as

$$\varepsilon_r = -\frac{1}{4}B^3 \rho g f \frac{H^3}{h} \tag{3}$$

where f is the wave frequency, h is the local water depth, and B is an adjustable parameter of order one.

The simple wave model used in this work includes the concept of a wave roller, an elevated body of turbulent water created by wave breaking and riding on the front face of the wave (Svendsen, 1984). The wave-roller energy flux is incorporated into the wave model to more accurately describe the cross-shore distribution of dissipation (Lippmann, Thornton, and Reniers, 1996b). In this wave model, the wave-roller energy flux gradient is given by $\partial/\partial x(E_r c_g \cos\alpha)$, where E_r is the energy in the wave roller. Incorporating the wave-roller term into the overall energy flux balance (Equation [2]) gives

$$\frac{\partial}{\partial x}\left(E_w c_g \cos\alpha\right) + \frac{\partial}{\partial x}\left(E_r c_g \cos\alpha\right) = -\frac{1}{4}B^3 \rho g f \frac{H^3}{h} \tag{4}$$

Equation (4) has been derived under the assumption that the energy transformation at a given location is represented by a single wave. In the real world, the wave field is comprised of a spectrum of random wave heights that break in a distribution that transforms across the surf zone. Thornton and Guza (1983) incorporated this concept into the energy flux balance by ensemble averaging the total wave field through the Raleigh distribution, $p(H)$, with a modified Raleigh distribution determined empirically to describe the breaking wave distribution, $p_b(H)$, such that

$$\left\langle \frac{\partial}{\partial x}\left(E_w c_g \cos\alpha\right)\right\rangle + \left\langle \frac{\partial}{\partial x}\left(E_r c_g \cos\alpha\right)\right\rangle = \left\langle -\frac{1}{4}B^3 \rho g f \frac{H^3}{h}\right\rangle \tag{5}$$

where <> indicates ensemble averaging. Carrying out the integration in the ensemble averaging operation in Equation (5) following Lippmann, Brookins, and Thornton (1996a) yields

$$\frac{\partial}{\partial x}\left(\frac{1}{8}H_{\mathrm{rms}}^2 c_g \cos\alpha\right) + \frac{3f\sqrt{\pi}}{4\tan\sigma}\frac{\partial}{\partial x}\left[MH_{\mathrm{rms}}^3 G\cos\alpha\right] = \frac{3\sqrt{\pi}}{42} fMG\frac{H_{\mathrm{rms}}^3}{h} \tag{6}$$

where H_{rms} is the root-mean-square wave height, γ is an energy saturation coefficient given by H_{rms}/h, $G = 1 - 1/\left(1 + [H_{\mathrm{rms}}/\gamma h]^2\right)^{5/2}$, and $M = 1 + \tanh(8[H_{\mathrm{rms}}/\gamma h - 1])$ is a weighting function defined by Whitford (1988). In Equation (6), we have used the concept of the wave roller parameterized by its geometry in which σ is the wave/roller interface angle (Deigaard, 1993; Svendsen, 1984).

The wave height distribution is then found using a simple forward-stepping algorithm

$$\left(E_w c_{gx}\right)_2 + \left(E_r c_{gx}\right)_2 = \langle \varepsilon_r \rangle \Delta x + \left(E_w c_{gx}\right)_1 + \left(E_r c_{gx}\right)_1 \tag{7}$$

where the H_{rms} value at the next shoreward profile location is found knowing the previous H_{rms} value and calculated dissipation (Thornton and Guza, 1983).

The wave model requires three user-defined variables γ, B, and σ. The parameter γ is a saturation constant (defined earlier) that is largely constrained by observation to values between 0.32 and 0.42 and is taken to be 0.38 following Lippmann, Brookins, and Thornton (1996a). B is a variable describing the fraction of the wave face covered by the wave roller and is given the constant value of 1. The final variable σ is the angle of the wave/roller interface and is an important adjustable parameter in the overall assimilation scheme. Changing the angle of the wave/roller interface spatially changes the distribution of dissipation (Lippmann, Thornton. and Reniers, 1996b) and was initially chosen at a value of 10°.

ASSIMILATION METHOD

In any image of the surf zone, spatial patterns of wave dissipation due to breaking over submerged topography are manifested visually as brightness (intensity) arising from

incident light reflecting off of foam and bubbles (Lippmann and Holman, 1989, 1990; Lippmann, Holman, and Hathaway, 1993). If image data are accurately transformed to an appropriate ground coordinate system, spatial patterns of time-averaged image pixel intensities can be scaled to be representative of true dissipation patterns (Aarninkhof and Ruessink, 2004). The strong correlation that exists between bathymetry and dissipation (Aarninkhof and Ruessink, 2004; Lippmann and Holman, 1989; Lippmann, Holman, and Hathaway, 1993), which can mathematically be related through a wave model (described previously), forms the basis of assimilation techniques (Van Dongeren, *et al.*, 2008). Assuming that the wave field dissipates all of its energy through the surf zone, image intensity values can be scaled by the offshore energy flux, E_{wo}, such that

$$E_{wo} = \int_0^\infty \langle \varepsilon_r \rangle \mathrm{d}x = \lambda \int_0^\infty \langle I \rangle \mathrm{d}x \quad (8)$$

where λ is a proportionality constant, allowing scaled image intensities to be quantitatively compared with dissipation numerically calculated by a wave model.

If the surf zone bathymetry is not initially known, it must be assumed and stitched seamlessly to the known subaerial and offshore profiles, and subsequently input into the wave model along with known offshore wave conditions (*i.e.,* H_{rms}, f, and α) to numerically predict initial dissipation distributions. A corresponding profile of image intensity is extracted from a time-averaged mosaic at the same alongshore location, scaled by offshore wave energy flux (Equation [8]), and compared along the cross-shore profile locally to the spatial distribution of dissipation calculated by the wave model. The initially estimated bathymetry can then be updated as a function of the difference between scaled image intensity and calculated dissipation in a manner that brings the two into closer agreement. Following Van Dongeren *et al.* (2008), in regions where the modeled dissipation is less or more than the scaled dissipation derived from the video data, the water depth is decreased or increased, respectively. This assimilation process is iteratively repeated until the difference between the scaled-image intensities and the modeled dissipation are within a user-defined range, at which point the assimilated bathymetry becomes the final estimate. The assimilated profiles can be quantitatively evaluated by comparing with actual measured profiles obtained with traditional *in situ* methods. Previous work using similar data assimilation techniques with land-based imagery to estimate bathymetry have produced results with typical root-mean-square (RMS) values around 30–50 cm (Van Dongeren *et al.*, 2008).

The assimilation routine begins by taking an assigned FRF profile data set with data removed from the surf zone and initially estimating the surf zone bathymetry, h, as a function of cross-shore coordinate, x, using the hyperbolic tangent equation (Equation [1]). This profile shape is used instead of a linear interpolation because the wave model was empirically found to achieve better results when it is forced to accrete rather than erode (following Van Dongeren *et al.*, 2008). Image intensity profiles are then selected from a time-averaged mosaic that overlays measured bathymetry profiles (as in Figures 3 and 4). A single bathymetric profile and all necessary parameters are input into the wave model, which calculates the wave dissipation. The intensity profile is scaled and compared with the dissipation profile calculated by the wave model.

The initially estimated bathymetry is then updated as a function of several factors. The first is the difference between image intensity and calculated dissipation that determines the magnitude of the change in bathymetry after each iteration. The magnitude of the update change is tapered as the distance seaward from the midpoint of the surf zone increases, thereby smoothly connecting the updated bathymetry to the seaward profile used as input to the model. In addition, the bathymetry update exponentially decreases at distances within a quarter of the profile length from the shoreline, again to smoothly connect the updated bathymetry to the known subaerial profile. This process is repeated for each profile in the data set until the difference between image intensity and modeled dissipation is acceptable on the basis of one of three criteria: (1) a maximum RMS dissipation difference value less than 10 W/m^2, (2) both a mean RMS difference less than 10 W/m^2 and an RMS difference less than 2 W/m^2 at the location of the peak intensity, or (3) 32 iterations. The RMS difference requirements between numerical dissipation and scaled intensities used to stop the assimilation routine were determined empirically to produce the best results.

RESULTS

Aerial video system overflights used in this study were conducted on 16 April 1999, 13 April 2002, and 16 January 2003. Field research facility bathymetry surveys from 19 April 1999, 17 April 2002, and 08 January 2003 were used as ground truth for the respective overflights. The wave dissipation estimated from an example scaled image intensity obtained on 13 April 2002 at alongshore location $y = 1$ m in the FRF coordinate system is shown in Figure 6. The modeled wave dissipation after the first model iteration over the initial (assumed) profile is also indicated in Figure 6. The modeled dissipation differs from the observed dissipation (from the scaled imagery) because of large differences (10s–100s cm) between the assumed featureless profile and the measured bathymetry. The magnitude of the difference between modeled and scaled dissipation is used to modify the bathymetry by scaling a set depth increment (for this work set at 0.25 m) by the dissipation difference divided by the scaled value. Thus, when the difference is small, the increment that the bathymetry is updated is also correspondingly small, typically on the order of a few centimeters. Subsequent model iterations run on the updated bathymetry create new modeled dissipation profiles and consequently new updated (assimilated) bathymetry. The value of the initial increment is arbitrarily set (*i.e.,* 0.25 m) and essentially sets the rate of initial convergence on the final profile. The iterations are stopped after the RMS difference fell below one of the three criteria described earlier.

The final assimilated depth profile (after 29 iterations) is compared with the actual measured bathymetry (Figure 7).

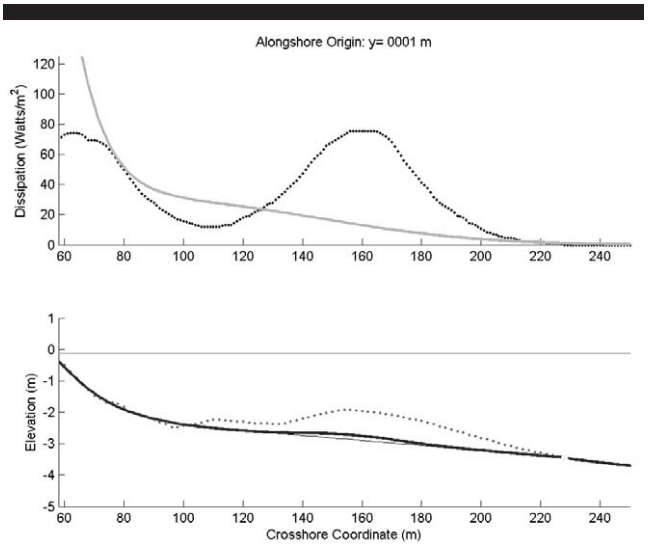

Figure 6. Top panel: wave dissipation (W/m^2) estimated from scaled image intensity (black dots) and after the first run of the wave model (solid line). Bottom panel: initial cross-shore bathymetric profile (thin solid line) and the first assimilation profile (thick solid line). Also shown in the bottom panel is the target (measured) profile inside the surf zone (dotted line) obtained at alongshore coordinate $y = 1$ m in the FRF coordinate system. The wave model is initialized in 8-m water depth about 800 m from shore. The foreshore and offshore parts of the profile are not shown for clarity.

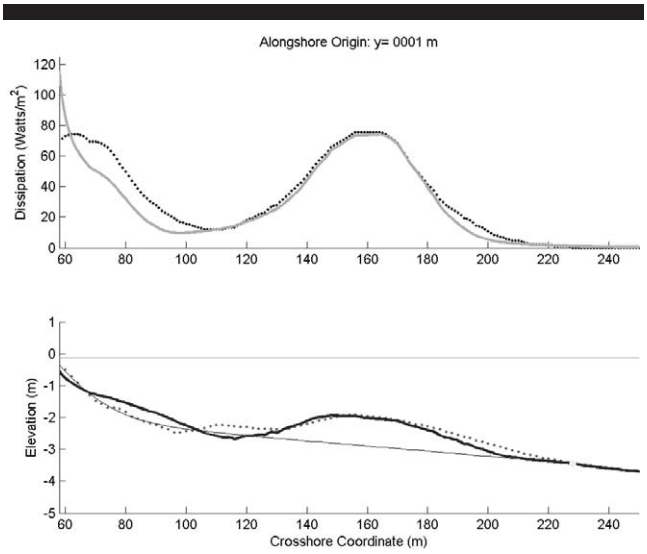

Figure 7. Top panel: wave dissipation (W/m^2) estimated from scaled image intensity (black dots) and after the last run of the wave model (solid line). Bottom panel: initial cross-shore bathymetric profile (thin solid line) and the final assimilation profile (thick solid line) after 29 iterations. Also shown in the bottom panel is the target (measured) profile inside the surf zone (dotted line) obtained at alongshore coordinate $y = 1$ m in the FRF coordinate system.

In about the middle of the surf zone in the vicinity of the sandbar location ($x = 160$ m), the modeled wave dissipation nearly matches that of the scaled image intensities. Consequently, the assimilated profile nearly matches the measured bathymetry. The differences in dissipation are larger near the shoreline where the wave model does not behave well because the model does not allow reflections or swash motions. The differences are also larger at the seaward edge of the surf zone ($x = 200$ m) where most of the wave breaking is initiated and the scaled image intensities are perhaps not as representative of dissipation as the model predicts; consequently the assimilated profiles are not as closely matched. In general, the overall shape of the measured profile is well represented by the assimilated profile, with RMS error for this profile of 17 cm. This profile is one of the best examples from the data used in the study.

For further analysis, individual assimilated profiles were triangularly interpolated onto an evenly spaced grid spanning the FRF survey region. These gridded data were plotted as contours (Figure 8) to examine the resolution of alongshore and larger-scale bathymetric features that are not visible or evident when looking at individual cross-shore profiles. Comparisons with the actual FRF surveyed bathymetry indicate that the assimilated data estimates well the variation in the larger-scale bathymetric features within the surf zone (with RMS difference of 0.26 m) and captures the large alongshore variation in sand bar elevation. Results from the other 2 days examined had RMS errors of 0.25 m and 0.35 m.

The RMS differences between measured profiles and assimilated bathymetry were calculated as a function of alongshore and cross-shore coordinates (Figure 9). The RMS differences between the initial (featureless) profile and the measured bathymetry show the spatial improvement in depth estimates using data assimilation. The cross-shore variability shows that over the sandbar there is a fourfold improvement in RMS differences, dropping from about 0.80 m to about 0.20 m. Near the shoreline, the improvement is minimal, primarily because the hyperbolic tangent fit (Equation [1]) used to fill in the artificial surf zone gap turns out to be a good representation of the actual profile near the shoreline (thus no improvement is necessary or realized). The alongshore variability shows marked increase in RMS errors around FRF alongshore coordinate $y = 500$ m. This location is very close to the large FRF research pier (Figure 3), and it is very likely that a combination of a lack of surveyed data in this region and inaccurate behavior of the wave model in the vicinity of the pier (where large seaward-flowing rip currents are known to persist) biased our estimate of the assimilated profile. The assimilated profiles clearly better represent the bathymetry than the featureless numerical profile that might be used with incomplete ALB profiles.

The effects of changing the initial parameters γ, B, and σ were tested to find values that optimized the capability of the assimilation routine. Average RMS errors for bathymetry were calculated over a range of σ values from 0.5 to 20° (Figure 10). Optimal results were found for $\sigma = 4°$, eventually used for all final analyses. In general, assimilated results were only weakly sensitive to the choice of σ ranging from 2 to 20°, with RMS errors varying only $\pm 1\%$ over this range. Testing of B and γ revealed that the assimilated results (not shown) were generally insensitive to the choice for B ranging

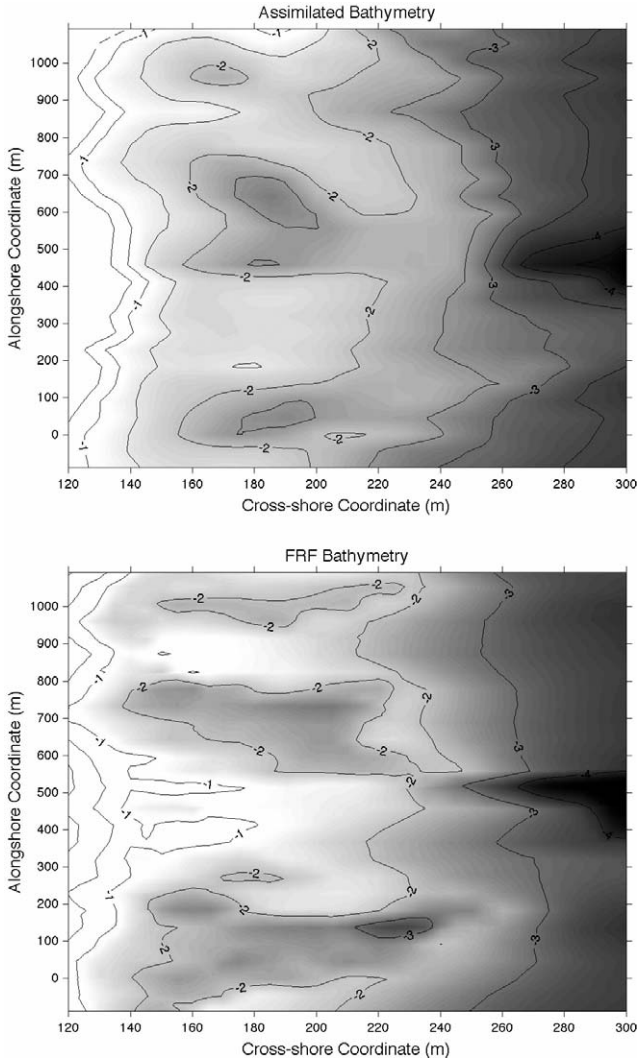

Figure 8. Contour plot of the assimilated bathymetry (top panel) from 13 April 2002 compared with the measured FRF bathymetry (bottom panel) from 17 April 2002. The local FRF coordinate system is the same as that shown in Figure 2. The assimilation reasonably approximates the surf-zone bathymetry with RMS difference of 0.26 m over the extent of the region.

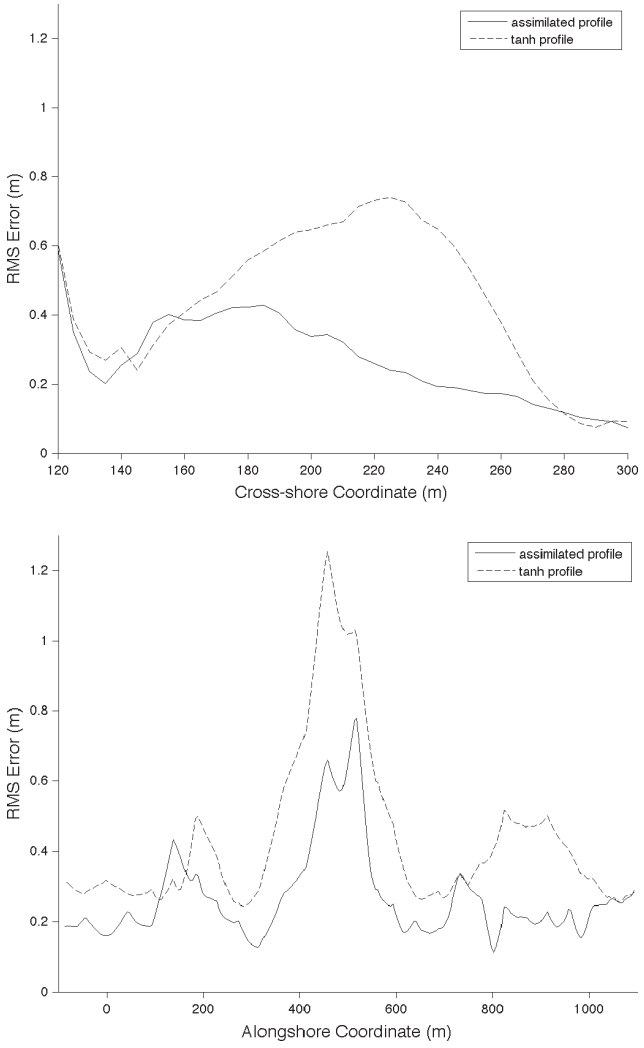

Figure 9. RMS difference between assimilated and measured bathymetry (solid lines) as a function of cross-shore (top panel) and alongshore (bottom panel) coordinates. Also shown for comparison are the RMS differences between the initial assumed profile on the basis of Equation (1) and the measured bathymetry (dashed lines). Data are from 13 April 2002. Largest differences occur near the shoreline (where the model performs poorly) and in the center region near the FRF pier (where the pier interferes with the airborne imagery, the bathymetry is not well surveyed, and the model does not account for the presense of the pier pilings).

from 0.5 to 1.5, and γ ranging from 0.32 to 0.42; thus, initial values used for these parameters were deemed acceptable.

DISCUSSION

The assimilation routine appears to work generally well, similar to studies with fixed, land-based video (Van Dongeren *et al.*, 2008) that found best results for cases with simple bathymetric profiles and where accretion of the initial bathymetry is the primary assimilation mode (although it is not clear why assimilation works better for accreting than eroding beach profiles). Adding terms to account for setup (the superelevation of the mean water surface) may improve the wave model's capability near the shoreline, where forcing the dissipation to zero in the current model is not realistic. Finally, the model parameters have all been calibrated to produce optimal results for the specific beach location and would likely need to be verified in other geographical locations.

The assimilation process is highly dependent on the quality of video data and the estimate of heading biases required for alignment of images that make up the mosaics. The image data from the AVS had synchronized GPS data, but did not provide any image orientation information, resulting in slightly blurred imagery with pitch, roll, and yaw biases that must be accounted for. The small deviations in pitch and roll between successive images are smoothed out during the averaging process, and thus do not negatively affect the final results. The biases associated with pitch and roll are

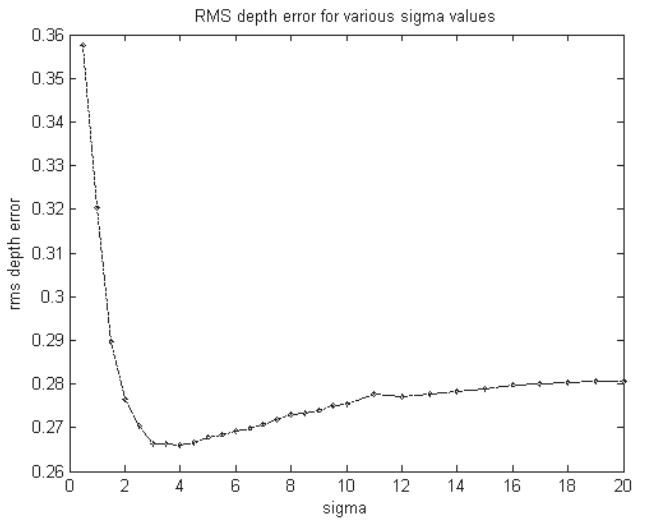

Figure 10. Total RMS difference as a function of σ from 13 April 2002. Optimal results are obtained with σ values near 4°. In general, the errors were relatively insensitive (1–2%) to σ values ranging 2–20°.

generally accounted for by checking the location of features visible in image mosaics with known ground coordinates to ensure proper alignment of the images with the shoreline position. Heading biases are accounted for manually, which allows mosaics to be created but significantly slows the analysis procedure. In some cases, the pitch, roll, and heading biases are not well constrained and cause dropouts in an otherwise continuous alongshore overflight pattern.

The bathymetric and AVS data were not collected on the same dates, thereby introducing some uncertainty into the final assimilated error analysis. The lag between the video overflights and the *in situ* surveys ranged between 3 and 8 days, enough time for the bathymetry to have evolved. In each of the three cases examined herein, the wave climate was relatively benign, with RMS wave heights less than 1 m, somewhat reducing the bathymetric change that might have occurred.

Although the input data used for this work did not come from LIDAR sources, the results suggest that such an assimilation technique could be used for estimating surf-zone bathymetry for incomplete ALB surveys. Time-averaged mosaics created from airborne video data showed results that are comparable with similar assimilation techniques that use land-based video systems, with average RMS errors ranging from 0.25 to 0.50 m (Van Dongeren *et al.*, 2008). Errors of this magnitude would allow for LSCB to be considered in regions where LIDAR systems cannot estimate the seabed elevation inside the surf zone or in regions where water turbidity is too high.

This study used uncompressed image data collected by an AVS system that operated at a higher altitude and lower speed than that of typical ALB systems that fly at relatively lower altitude and higher speed. The altitude and the speed rate of the ALB system can result in video images with insufficient image overlap required for creation of time-averaged image mosaics. For the digital video data to be useful for bathymetry assimilation procedures, individual ground features must have a longer dwell time than currently provided. Imagery collected by ALB systems does, however, have much more accurate GPS/INS synchronization than the video data used in this work. It is highly likely that the use of video data obtained concurrently with ALB would improve image georeferencing and eliminate the need to manually adjust images for mosaic alignment, potentially reducing error in final bathymetry estimates.

Obtaining initial offshore wave conditions is essential to the assimilation methods, potentially limiting the area of usefulness of assimilation techniques to locations where such data are collected or where accurate wave forecasting models can be relied upon. The potential to gather this type of information from ALB sea-surface return data could make the process autonomous, giving it the capability to operate anywhere.

CONCLUSIONS

This work presents a data assimilation technique that can support ALB surveys by estimating bathymetry in highly turbid nearshore regions (including the surf zone) using aerial imagery where ALB surveys are currently unsuccessful. The assimilation is accomplished by comparing spatial wave dissipation patterns extracted from time-averaged airborne imagery with dissipation values produced by a simple wave-energy transformation model. An initial bathymetry is assumed in the surf zone between known subaerial beach topography and the offshore profile. Differences between modeled dissipation and observed image pixel intensity patterns are minimized by incrementally modifying the bathymetry. Assimilated bathymetric profiles along the North Carolina coastline from three overflight missions using an AVS are compared with bathymetric data collected using traditional *in situ* methods at the USACEFRF in Duck, NC. Root-mean-square differences between assimilated and measured bathymetry range from 0.25 to 0.35 m, similar to assimilation methods based on land-based imagery (Van Dongeren *et al.*, 2008). Uncertainties of this magnitude are acceptable for studies of LSCB or for general wave modeling in the nearshore environment. Successful application of the assimilation methods will increase the usefulness of present airborne LIDAR bathymetry systems to regions where wave breaking occludes bottom signals from being collected.

ACKNOWLEDGMENTS

This research was generously supported by the Joint Airborne Lidar Bathymetry Technical Center of Expertise. The bathymetric and wave data were graciously provided by the staff of the USACE FRF in Duck, NC. The overflight missions were expertly piloted by Dean Morris of Flywright Aviation, Inc., out of Manteo, NC.

LITERATURE CITED

Aarninkhof, S. G. J. and Ruessink, B. G., 2004 Video observations and model predictions of depth-induced wave dissipation. *IEEE Transactions on Geoscience and Remote Sensing,* 42, 2612–2622.

Aarninkhof, S.G.J.; Ruessink, B.G., and Roelvink, J.A., 2005. Nearshore subtidal bathymetry from time-exposure video images. *Journal of Geophysical Research,* 110, C09011, doi:10.1029/2004JC002791.

Birkemeier, W.A. and Mason, C., 1984. The CRAB: a unique nearshore surveying vehicle. *Journal of Surveying Engineering,* 110(1), 1–7.

Deigaard, R., 1993. A note on the three-dimensional shear stress distribution in dissipative water waves. *Coastal Engineering,* 20, 157–171.

Guenther, G.C., 2001. Airborne LIDAR bathymetry. *In:* Maune, D.F. (ed.), *Digital Elevation Model Technologies and Applications: The DEM Users Manual*. Bethesda, Maryland: American Society fo r Photogrammetry and Remote Sensing, pp. 236–306.

Holland, K.T.; Holman, R.A.; Lippmann, T.C.; Stanley, J., and Plant, N., 1997. Practical use of video imagery in nearshore oceanographic field studies. *IEEE Journal of Oceanic Engineering, Special Issue of Image Processing for Oceanic Applications,* 22(1), 81–92.

Irish, J.L.; McClung, J.K., and Lillycrop, W.J., 2000. Airborne LIDAR bathymetry: the SHOALS system. *PIANC Bulletin,* 103, 43–53.

Kannan, S.; Lippmann, T.C., and List, J.H., 2003. The relationship of nearshore sandbar configuration to shoreline change. *In: Proceedings of the International Conference on Coastal Sediments 2003* (Clearwater, Florida), pp. 1–7.

LeMahaute, B., 1962. On nonsaturated breakers and the wave run-up. *In: Proceedings of the 8thInternational Conference on Coastal Engineering* (Mexico City, Mexico, ASCE), pp. 77–92.

Lippmann, T.C.; Brookins, A.H., and Thornton, E.B., 1996a. Wave energy transformation on natural profiles. *Coastal Engineering,* 27, 1–20.

Lippmann, T.C.; Herbers, T.H.C., and Thornton, E.B., 1999. Gravity and shear wave contributions to nearshore infragravity motions. *Journal of Geophysical Research,* 29(2), 231–239.

Lippmann, T.C. and Holman, R.A., 1989. Quantification of sand bar morphology: a video technique based on wave dissipation. *Journal of Geophysical Research,* 94(C1), 995–1011.

Lippmann, T.C. and Holman, R.A., 1990. The spatial and temporal variability of sand bar morphology. *Journal of Geophysical Research,* 95(C7), 11575–11590.

Lippmann, T.C.; Holman, R.A., and Hathaway, K.K., 1993. Episodic, nonstationary behavior of a double bar system at Duck, NC, U.S.A., 1986–1991. *Journal of Coastal Research,* 15, 49–75.

Lippmann, T.C. and Kannan, S., 2003. Observations of large-scale alongshore variability in nearshore sandbars. In: *Proceedings of the International Conference on Coastal Sediments 2003* (Clearwater, Florida), pp. 1–7.

Lippmann, T.C.; List, J.H., and Kannan, S., 2003. Shoreline response to storms and the configuration of nearshore bars. *In: Proceedings of the 29thInternational Conference on Coastal Engineering* (Cardiff, Wales, ASCE), pp. 2792–2799.

Lippmann, T.C.; Thornton, E.B., and Reniers, A.J.H.M., 1996b. Wave stress and longshore currents on barred profiles. *In:* Dally, W. (ed.), *Proceedings of Coastal Dynamics '95: International Conference on Coastal Research in Terms of Large Scale Experiments* (Gdansk Poland, ASCE), pp. 401–412.

Morris, T.M., 1966. *Manual of Photogrammetry,* Volume I, 3rd edition. Falls Church, Virginia: American Society of Photogrammetry, p. 536.

Svendsen, I.A., 1984. Wave heights and setup in a surf zone. *Coastal Engineering,* 8, 303–329.

Thornton, E.B. and Guza, R.T., 1983. Transformation of wave height distribution. *Journal of Geophysical Research,* 88, 5925–5938.

Van Dongeren, A.; Plant, N.; Cohen, A.; Roelvink, D.; Haller, M., and Catalan, P., 2008. Beach Wizard: nearshore bathymetry estimation through assimilation of model computations and remote observations. *Coastal Engineering,* 55(12), 1016–1027.

Whitford, D.J., 1988. Wind and Wave Forcing of Longshore Currents across a Barred Beach. Monterey, California: Naval Postgraduate School, Ph.D. thesis, 205p.

Worley, C.R.; Lippmann, T.C.; Haines, J.W., and Sallenger, A.H., 1997. An aerial video system for rapidly measuring the spatial variability of very large scale (10^1–10^3 km) sand bar morphology. *In: Proceedings of the 3rd Coastal Dynamics Conference* (Plymouth, England), pp. 1–8.

Worley, C.R.; Lippmann, T.C.; Haines, J.W., and Sallenger, A. H., 1998. The spatial variability of largescale sand bars. *In: Proceedings of the 29thInternational Conference on Coastal Engineering* (Lisbon, Portugal, ASCE), pp. 1–12.